Spin-wave excitations in finite rectangular elements of Ni$_{80}$Fe$_{20}$

C. Bayer,* J. Jorzick, and B. Hillebrands
*Fachbereich Physik and Forschungsschwerpunkt MINAS, Technische Universität Kaiserslautern, Erwin-Schrödinger-Straße 56,
67663 Kaiserslautern, Germany*

S. O. Demokritov
Institut für Angewandte Physik, Westfälische Wilhelms-Universität Münster, Corrensstrasse 2-4, 48149 Münster, Germany

R. Kouba, R. Bozinoski, and A. N. Slavin
Department of Physics, Oakland University, Rochester, Michigan 48309, USA

K. Y. Guslienko
Materials Science Division, Argonne National Laboratory, 9700 S. Cass Avenue, Argonne, IL 60439, USA

D. V. Berkov and N. L. Gorn
INNOVENT e.V. Jena, Pruessingstraße 27B, D-07745, Jena, Germany

M. P. Kostylev
*St. Petersburg Electrotechnical University, 197376 St. Petersburg, Russia, and Fachbereich Physik and Forschungsschwerpunkt MINAS,
Technische Universität Kaiserslautern, Erwin-Schrödinger-Straße 56, 67663 Kaiserslautern, Germany*

A Brillouin light scattering study and theoretical interpretation of spin-wave modes in arrays of in-plane magnetized micron-size rectangular Ni$_{80}$Fe$_{20}$ elements are reported. It is shown that two-dimensional spin-wave eigenmodes of these elements can be approximately described as products of one-dimensional spin-wave eigenmodes of longitudinally and transversely magnetized long finite-width permalloy stripes. The lowest eigenmodes of rectangular elements are of dipole-exchange nature and are localized near the element edges, while the higher eigenmodes are of a mostly dipolar nature and are weakly localized near the element center. The frequency spectra and spatial profiles of these eigenmodes are calculated both analytically and numerically, and are compared with the results of the Brillouin light scattering experiment.

I. INTRODUCTION

Recent developments in the field of magnetic storage and magnetic sensors created a lot of interest in the dynamic properties of small magnetic elements made by patterning magnetic films and multilayers.[1,2] Growing demand for higher lateral density in magnetic recording and for higher speed of memory operation focused the attention of many researchers on the spin dynamics of thin-film (several tens of nanometers) magnetic elements with lateral dimensions of $0.1-1$ μm operating in the microwave frequency range $(3-30$ GHz). It turns out that the frequencies and wavelengths of dipole-exchange spin waves (that happen to be the dynamic eigenexcitations of nanosized magnetic elements) lie in these frequency and spatial intervals. Thus, the understanding of spin-wave eigenexcitations of small magnetic elements is of critical importance both for fundamental reasons and for the modern applications in magnetic recording and sensor technology. The problem is not trivial: for the magnetic elements in question both dipole-dipole and exchange interactions should be taken into account simultaneously when dynamic properties of the elements are analyzed. An additional difficulty is created by the fact that in most cases these small magnetic elements (e.g., thin rectangular prisms) have a nonellipsoidal shape and, therefore, the magnetic field

inside such elements is strongly inhomogeneous when a homogeneous external magnetic bias field is applied.

These particular circumstances result in several characteristic properties of magnetic excitations in these elements that have been recently observed in experiments: quantization of spin-wave frequencies in longitudinally magnetized magnetic stripes and tangentially magnetized magnetic discs,[3–8] and localization of spin-wave modes in the regions of inhomogeneous internal magnetic field (spin-wave wells) in transversely magnetized magnetic stripes and rectangular elements.[9–11]

The study of quantized and localized spin-wave modes of small magnetic elements is very important from yet another point of view. Each finite-size magnetic element can be considered as a magnetic resonator having eigenfrequencies in the microwave frequency range and, therefore, having maxima in the thermal noise spectrum near these eigenfrequencies (or resonance frequencies). If this element is used as a part of a magnetic reading head, or as a memory element at microwave frequencies (and a typical speed of a modern computer processor is around $3-4$ GHz) it is the thermal magnetic noise that limits the figures of merit of those devices.[12–14] Recently, the pronounced maxima in the thermal noise spectrum of small magnetic elements has been observed experimentally in the microwave frequency range

as well as addressed theoretically.[12–14] Thus, to understand this effect and to be able to control the high-frequency properties of small magnetic elements it is necessary to study the properties of thermally excited spin-wave modes in laterally confined magnetic elements.

If the shape of a small magnetic element is ellipsoidal the spin-wave spectrum of the element can be calculated analytically,[15,16] and for many decades the experimentally studied magnetic elements relevant for applications were approximated by ellipsoidal elements with corresponding demagnetizing factors.[17] In reality, the magnetic elements used in applications have, for the most part, nonellipsoidal shape which leads to the substantial inhomogeneity of their internal magnetic field. It has been found recently that the nonellipsoidal shape of these elements drastically affects their dynamic properties.

In the experimental part of this paper we show that in thin rectangular magnetic elements both the quantization of spin-wave modes due to the finite in-plane sizes of the element and the localization of these modes due to the inhomogeneity of the internal bias magnetic field manifest themselves simultaneously. In the theoretical part, we introduce a simple approximate analytical approach which allows us to describe both the quantization and localization effects observed in thin in-plane magnetized rectangular magnetic elements. In the numerical part of the paper the approximate results of our analytical approach are verified by direct micromagnetic simulations and are compared to the results of the Brillouin light scattering (BLS) experiment.

Our analytical approach is based on the approximate representation of the two-dimensional dynamic magnetization distributions as a product of two one-dimensional magnetization distributions corresponding to the eigenmodes of infinitely long longitudinally and transversely magnetized magnetic stripes having finite widths. In the case of a longitudinally magnetized long stripe the one-dimensional eigenmodes along the stripe width are calculated using the approximate dipolar boundary conditions obtained in Ref. 18.

In the case of a transversely magnetized stripe (or stripe magnetized along its width) the main qualitative effects are caused by a strongly inhomogeneous static internal magnetic field. This inhomogeneity causes the creation of a so-called "spin-wave well" (SWW).[9–11] The one-dimensional eigenmodes along the stripe width in this case are calculated using the Mathieu function formalism,[19] or using the approximate theory presented in Ref. 20 or by numerical solution of a one-dimensional integral equation describing the dipole-exchange spin-wave modes in an inhomogeneous bias magnetic field.

To check the results of the above described approximate analytical methods for thin rectangular magnetic elements we performed numerical simulations of two types: thermodynamic simulations based on Langevin dynamics, and field pulse simulations at zero temperature based on the object-oriented micromagnetic framework[21] (OOMMF).

It should be also mentioned, that recently performed numerical calculations[22–24] of the frequencies of normal modes in rectangular permalloy prisms made by a different method
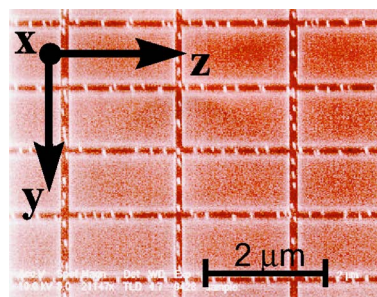

FIG. 1. SEM image of an array of magnetic rectangular elements with used coordinate system.

gave results that quantitatively coincide with the results of our approximate analytic formalism (see Fig. 8 in Ref. 22).

II. SAMPLES AND EXPERIMENTAL SETUP

The investigated samples were prepared from permalloy ($Ni_{80}Fe_{20}$) films, thermally evaporated on Si(111) substrates in UHV. Patterning was performed by means of electron beam lithography and ion beam etching. The rectangular elements were prepared with lateral dimensions of $1 \times 1.75 \ \mu m^2$, a thickness of 35 nm, and an element spacing of 0.1 μm. The elements were arranged in arrays of dimensions of $500 \times 500 \ \mu m^2$. The high quality of the patterning process has been confirmed by atomic force microscopy (AFM) and scanning electron microscopy (SEM), as illustrated in Fig. 1. As it is seen from Fig. 1, the used technique guaranties a high quality patterning process, which provides a very good flatness of the stripe boundaries and reproducibility of the stripe widths.

The spin-wave spectrum of a confined system can be investigated by various techniques: ferromagnetic resonance,[25] time resolved Kerr magnetometry,[11,26–28] and Brillouin light scattering spectroscopy (BLS).[29] The BLS experimental technique has a number of advantages for the investigation of patterned magnetic structures. It combines the possibility to study the dynamics of patterned systems in the frequency range of up to 100 GHz (corresponding time resolution is 10 ps) with a high lateral resolution of $20-30 \ \mu m$ defined by the size of the laser beam focus. Moreover, BLS can be used in the so-called "Fourier microscope" mode with an effective resolution below 200 nm.[6] Another important advantage of BLS is its very high sensitivity which allows us to register thermally excited spin-wave modes, so the coherent excitation of the element by an external signal is not necessary. This property of BLS is especially useful for the experimental investigations of complicated, strongly confined spin-wave modes in patterned magnetic elements having nonellipsoidal shape as the coherent excitation of such modes is not easy.

The BLS process in bulk magnetic samples and magnetic films is discussed in detail in Refs. 6,29: monoenergetic photons (visible light, usually green line of an Ar^+ laser, 514.5 nm) with the wave vector $\mathbf{q}_I$ and frequency $\omega_I = cq_I$ interact with the elementary quanta of spin waves (magnons), characterized by the magnon wave number $\mathbf{q}$ and fre-

quency ω. Because of the conservation laws resulting from the time- and space-translation invariance of the system the scattered photon gains an increase or decrease in energy and momentum if a magnon is annihilated or created:

$$\hbar\omega_S = \hbar(\omega_I \pm \omega), \tag{1}$$

$$\hbar\mathbf{q}_S = \hbar(\mathbf{q}_I \pm \mathbf{q}). \tag{2}$$

Measuring the frequency shift of the scattered light one obtains the frequency of the spin wave participating in the BLS process. From Eq. (2) it is evident, that the wave vector $\mathbf{q}_S - \mathbf{q}_I$, transferred in the scattering process, is equal to the wave vector $\mathbf{q}$ of the spin wave. Varying the scattering geometry one can sweep the value of q and measure the corresponding frequency ω. Thus, the spin wave dispersion $\omega(q)$ can be studied. At room temperature $(T_R \gg \hbar\omega/k_B \approx 1K)$ the annihilation and creation of a magnon have about the same probability.

It was shown in Ref. 6 that the intensity of the scattered light as a function of the transferred wave vector $\mathbf{q}$ is connected with the profile of the dynamic magnetization $m(\boldsymbol{\rho})$ of a spin-wave mode confined in the element:

$$I(\mathbf{q}) \propto \left| \int m(\boldsymbol{\rho}) \cdot \exp(-i\mathbf{q}\boldsymbol{\rho}) d\boldsymbol{\rho} \right|^2. \tag{3}$$

Thus, the light scattering intensity is proportional to the squared Fourier transform of the dynamic magnetization $m(\boldsymbol{\rho})$, where $\boldsymbol{\rho} = y\mathbf{e}_y + z\mathbf{e}_z$. If BLS is used in the "Fourier microscope" mode, the light scattering intensity is measured as a function of $\mathbf{q}$. On the basis of this information the mode profile $m(\boldsymbol{\rho})$ in the elements is reconstructed. In the "Fourier microscope" mode the spatial resolution δ is determined by the accessible transferred wave vector interval $\pi/\Delta q$. For BLS experiments in the backscattering geometry it follows that $\Delta q = 2q_I$ and $\delta = 120-130$ nm for the green Ar$^+$ laser line.

III. EXPERIMENTAL RESULTS

In our previous experiments the spectrum of spin-wave modes standing along the finite width of a long magnetic stripe was investigated. For these long stripes two different geometries can be considered and they give a possibility to investigate two different effects separately.

In the first geometry the applied magnetic field is along the stripe length and, therefore, the internal magnetic field is homogeneous and equal to the applied external magnetic field. In this case the wave vectors of the standing spin-wave modes of the stripe are directed along the stripe width and are perpendicular to the bias magnetic field, thus creating the conditions for the quantization of the Damon-Eshbach-like spin waves. The quantization is caused by the the physical boundaries of the stripe, i.e., spatial confinement of the standing spin-wave modes exists due to a finite width of the stripe.[5–7] Therefore, in the following this orientation of the bias magnetic field will be called the Damon-Eshbach geometry.

The second geometry corresponds to the case when the applied magnetic field and the static magnetization $\mathbf{M}_S$ are
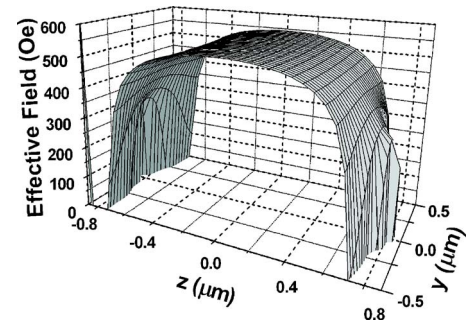

FIG. 2. Plot of the z component of the effective magnetic field of a rectangular element with the width $w=1$ μm, length $l = 1.75$ μm, and thickness of $L=35$ nm calculated using OOMMF (Ref. 21). The external bias magnetic field of 600 Oe was oriented along the length l of the rectangular magnetic element. Note, that the effective field calculated with OOMMF is negative near the edges $z=\pm l/2$ of the element, due to the definition of the exchange field (Ref. 31). Here for clarity we show only the positive values of the internal bias field. The corresponding distribution of static magnetization is shown in Fig. 10.

directed along the width of a thin stripe. Since in a continuous magnetic film waves with $\mathbf{q}\|\mathbf{M}_S$ are called magnetostatic backward volume waves (MSBVW), we refer to this experimental geometry as the MSBVW geometry.

In this geometry, both the static and dynamic internal magnetic fields are strongly inhomogeneous along the stripe width. Nevertheless, for a large enough magnitude of the applied field the static magnetization is parallel to the bias field within almost the entire stripe. The strong demagnetization effect present in this geometry leads to the decrease of the static internal magnetic field near the stripe edges. A detailed analysis shows that the internal static field H_i has a broad maximum in the center of the stripe while it is vanishing completely near the edges of the stripe,[30] so the internal bias magnetic field is positive on the effective width l^* that is slightly smaller than the physical width l of the stripe. This inhomogeneity of the static internal field qualitatively changes the spatial profile of the lowest spin-wave modes in the stripe, and creates so-called "spin-wave wells" (SWW's) near the edges of the stripe, where the lowest spin wave eigenmodes of the stripe are localized.[9,11,10]

The rectangular magnetic elements with two finite in-plane sizes considered here are substantially nonellipsoidal. Thus, there is no orientation of the external bias field which provides a homogeneous static internal magnetic field inside a rectangular element. Figure 2 shows the distribution of the internal static magnetic field inside a rectangular magnetic element magnetized by the applied bias field of 600 Oe directed along the long side of the element. This distribution was obtained using micromagnetic simulations as discussed below.[21] It is calculated for rectangular permalloy elements with the width $w=1$ μm, length $l=1.75$ μm, and the thickness of $d=35$ nm used in our experiments. It can be seen, that the inhomogeneity of the internal bias field occurs mainly along the direction of the applied field (z direction). The inhomogeneity perpendicular to the applied field (y direction) is not so pronounced.

This property of the internal field profile suggests that two-dimensional distributions of the variable magnetization
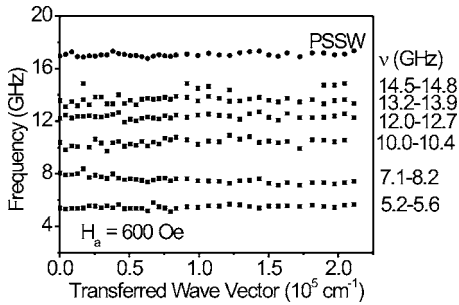
FIG. 3. Frequencies of spin-wave modes of an array of rectangular $1 \times 1.75 \, \mu m^2$ elements in an applied bias field of 600 Oe directed along the long side of the elements measured by BLS as a function of the transferred wave vector (which was also oriented along the length of the elements).

in the spin wave eigenmodes of a rectangular magnetic element can be treated as a product of the one-dimensional eigenmodes of a longitudinally and a transversely magnetized long stripe discussed above. This approach will be described in detail in the theoretical part of the paper.

Figure 3 shows the experimentally measured frequencies of the spin-wave eigenmodes of such an element. Here both the applied field and the transferred wave vector are directed along the long side (length) of the element. It must be noted, that although the wave vector of light in the BLS experiment shown in Fig. 3 was directed along the length of the rectangle (and, therefore, along the bias magnetic field) due to the finite aperture of the objective lens of our BLS setup we were able to probe the total resulting magnitude of the wave vector of the spin-wave modes of the element. This total mode wave vector has components both along and perpendicular to the bias magnetic field due to fact that our rectangular magnetic elements have two finite in-plane sizes. This property of our BLS setup is of much smaller importance in the case of experiments in magnetic stripes where the length of the stripe is much larger than its width. When the direction of the wave vector of light in our experiments was chosen parallel to the short side (width) of the magnetic element the observed frequencies of the spin-wave modes were the same as in Fig. 3, but the observed relative mode intensities were different. By recording the BLS intensity of a given mode as a function of the transferred wave vector when this wave vector is first directed along the length and then along the width of the rectangular element, it is possible to perform a two-dimensional "Fourier mapping" of the spin-wave modes in the element. This two-dimensional mapping helps to determine the structure and the spatial distribution of different modes.

As an example, Fig. 4 shows the BLS intensity of two spin-wave modes as a function of the absolute value of the transferred wave vector that is either parallel (circles) or perpendicular (squares) to the applied field and the static magnetization. It is evident, that the intensity distributions are completely different in these two cases. For the lowest spin-wave mode and a transferred wave vector parallel to the applied magnetic field (circles) an almost constant BLS intensity of the mode over a wide interval of wave vectors indicates a strong localization of this mode in real space
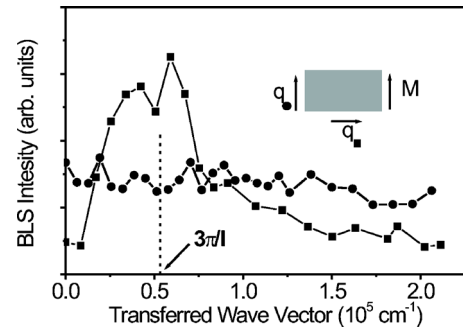

FIG. 4. BLS intensity of spin-wave modes in rectangular elements magnetized along their width. The points marked by circles show the intensity of the lowest spin-wave mode in the case when the transferred wave vector was directed along the applied magnetic field. The points marked by squares show the intensity of the third spin-wave mode in the case when the transferred wave vector was directed perpendicular to the bias magnetic field. Note, that the applied field in this special case was directed along the short side (width) of the element.

along the direction of the bias magnetic field.

Contrary to that, for the third spin-wave mode and a transferred wave vector perpendicular to the bias field the mode intensity has a maximum around $k = 3\pi/l$ and, therefore, the third mode, probably, occupies the whole length of the rectangle and has two nodes along the rectangle length. Thus, the spatial mode structure can be approximately determined from the above described two-dimensional "Fourier-mapping" of the mode intensities done using BLS.

IV. APPROXIMATE THEORY OF SPIN-WAVE MODES IN A RECTANGULAR MAGNETIC ELEMENT

Let us consider a rectangular magnetic element schematically shown in Fig. 5. Note, that in all the considered geometries the x direction is perpendicular to the film plane, while the z axis is parallel to the applied magnetic field.

We assume that the element is magnetized to saturation by the external field $\mathbf{H}_e = H_e \mathbf{e}_z$ that is parallel to one of the in-plane sides of the rectangular element as shown in Fig. 5, so that the static magnetization in the elements is constant $\mathbf{M}_{stat} = M_S \mathbf{e}_z = const$ everywhere, except in the narrow regions situated near the element edges that are perpendicular to the
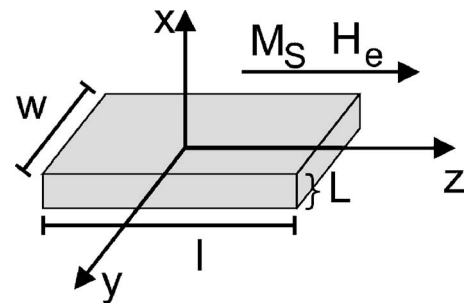

FIG. 5. Coordinate system for a considered rectangular magnetic element. The direction of static magnetization $\mathbf{M}_S$ and external field $\mathbf{H}_e$ is also indicated.

applied field (edge domains). Both crystalline and surface anisotropy of the material are neglected, which is a good approximation for permalloy.

Since we are interested in the linear oscillations of the magnetization, we assume that the component of the variable magnetization m_z directed along the field $\mathbf{H}_e$ (and the static magnetization $\mathbf{M}_{\text{stat}}$) is much smaller than the transverse components $m_z \ll m_x, m_y$ so the magnetization vector has the form

$$\mathbf{M}(\mathbf{r}) = m_x(\mathbf{r})\mathbf{e}_x + m_y(\mathbf{r})\mathbf{e}_y + M_S\mathbf{e}_z, \qquad (4)$$

where

$$\mathbf{r} = x\mathbf{e}_x + \boldsymbol{\rho} = x\mathbf{e}_x + y\mathbf{e}_y + z\mathbf{e}_z. \qquad (5)$$

Further, we assume that the element is thin and we will be interested in the lowest spin-wave modes having the uniform distribution of the variable magnetization along the $\mathbf{e}_x$ axis, i.e., $\mathbf{M}(\mathbf{r}) \rightarrow \mathbf{M}(\boldsymbol{\rho})$, where $\boldsymbol{\rho} = y\mathbf{e}_y + z\mathbf{e}_z$.

To calculate the spectrum of spin waves in the element we can use the formalism of tensorial Green's functions developed for infinite in-plane magnetized films in Refs. 32. In the framework of this formalism the linearized Landau-Lifshitz equation of motion for the magnetization and the Maxwell equations in the magnetostatic limit are reduced to an integral-differential equation for the vector amplitude $\mathbf{m}(\boldsymbol{\rho})$ $= m_x(\boldsymbol{\rho})\mathbf{e}_x + m_y(\boldsymbol{\rho})\mathbf{e}_y$ of the dynamic variable magnetization $\mathbf{m}(\boldsymbol{\rho}, t) = \mathbf{m}(\boldsymbol{\rho})\exp(i\omega t)$,

$$[-\alpha\omega_M\nabla_{\boldsymbol{\rho}}^2 + \omega_{H_i}(\boldsymbol{\rho})]\hat{\mathbf{I}} \cdot \mathbf{m}(\boldsymbol{\rho}) + i\omega\hat{\mathbf{T}} \cdot \mathbf{m}(\boldsymbol{\rho})$$

$$- \omega_M \int d\rho' \hat{\mathbf{G}}_{x,y}(\boldsymbol{\rho}, \boldsymbol{\rho}')\mathbf{m}(\boldsymbol{\rho}') = 0, \qquad (6)$$

where

$$\hat{\mathbf{I}} = \begin{bmatrix} 1 & 0 \\ 0 & 1 \end{bmatrix}, \quad \hat{\mathbf{T}} = \begin{bmatrix} 0 & -1 \\ 1 & 0 \end{bmatrix}, \hat{\mathbf{G}}_{x,y} = \begin{bmatrix} G_{xx} & G_{xy} \\ G_{yx} & G_{yy} \end{bmatrix},$$

$$\mathbf{m} = \begin{pmatrix} m_x \\ m_y \end{pmatrix} \qquad (7)$$

and $\omega_M = \gamma 4\pi M_S$, $\alpha = A/2\pi M_S^2$ is the exchange constant measured in cm^2, $\nabla_{\boldsymbol{\rho}}^2 = \partial^2/\partial y^2 + \partial^2/\partial z^2$:

$$\omega_{H_i}(\boldsymbol{\rho}) = \gamma H_i(\boldsymbol{\rho}), \qquad (8)$$

where

$$H_i(\boldsymbol{\rho}) = H_e - N_{zz}(\boldsymbol{\rho}) \cdot 4\pi M_S, \qquad (9)$$

and the coordinate-dependent demagnetizing factor for a rectangular prism

$$N_{zz}(\boldsymbol{\rho}) = -\int d\boldsymbol{\rho}' G_{zz}(\boldsymbol{\rho}, \boldsymbol{\rho}') \qquad (10)$$

was first calculated by Joseph and Schlömann in Ref. 17.

The components of the tensorial dipolar Green's function for a rectangular element have the following form:

$$G_{\alpha\beta}(\boldsymbol{\rho}, \boldsymbol{\rho}') = -\frac{1}{2\pi}\frac{\partial^2}{\partial\alpha\partial\beta'}R\left(\frac{|\boldsymbol{\rho} - \boldsymbol{\rho}'|}{L}\right), \qquad (11)$$

where $R(\xi) = \sinh^{-1}(1/\xi) + \xi - \sqrt{1 + \xi^2}$ and $\alpha, \beta = y, z$:

$$G_{xx}(\boldsymbol{\rho}, \boldsymbol{\rho}') = \frac{1}{2\pi L}\left[\frac{1}{\sqrt{L^2 + (\boldsymbol{\rho} - \boldsymbol{\rho}')^2}} - \frac{1}{|\boldsymbol{\rho} - \boldsymbol{\rho}'|}\right]. \qquad (12)$$

In Eq. (6) the first term describes inhomogeneous exchange interaction. The second term $\omega_{H_i}(\rho)$ describes the coordinate-dependent static demagnetization field inside the nonellipsoidal rectangular magnetic element. The term containing ω comes from the time derivative term in the Landau-Lifshitz equation, while the last integral term describes the dynamic demagnetizing field in the element.

The two-dimensional integral-differential equation (6) for the magnetization amplitude $\mathbf{m}(\boldsymbol{\rho})$ could be, in principal, solved numerically, but this solution is rather complicated. In fact, this solution is not substantially simpler than a direct numerical calculation of spin-wave modes using a micromagnetic approach that will be described below in Sec. V. Thus, for practical calculations we shall use a much simpler approximate analytical approach that uses the fact that the thickness of our rectangular magnetic element is much smaller than its in-plane sizes.

We would like to stress, that all our calculations of the spin-wave modes were made under the assumption that everywhere in the stripe the magnetic material is magnetized to saturation and the direction of the static magnetization is parallel to the direction of the applied field. This assumption, strictly speaking, is correct only for a very strong external field comparable in magnitude to the static magnetization of the material. In a small applied field, comparable to the demagnetizing field in the center of the stripe, the magnetization will rotate across the whole width of the stripe.[33] For moderate external fields below the demagnetizing field at the edges of the stripe there will be "edge domains," or regions where the effective internal field vanishes and the static magnetization rotates. The spin-wave modes in a transversely magnetized stripe in the case of the inhomogeneous magnetization were discussed in Refs. 33–36. Furthermore, we do not consider interelement magnetostatic coupling in our calculation as it has an influence on the spin-wave spectrum which is smaller than the accuracy of the approximate analytical approach.[37]

A. Approximate analytical approach

As was mentioned above, we only deal with the case when the rectangular magnetic element shown in Fig. 5 is thin, so that both aspect ratios of this element are small $L/l \ll 1$, $L/w \ll 1$. It is known that the matrix elements of the dipole-dipole interaction, that determine the dipolar part of the spin-wave dispersion in the element, are proportional to these aspect ratios (L/l or L/w) and are also small (see, e.g., Ref. 18,19,20). Thus, for the approximate calculation of the spin-wave mode frequencies the exact form of the dipole-dipole matrix element is not important, and we can use for that purpose the dipole-exchange dispersion equation of a continuous magnetic film [see Eq. (45) in Ref. 32], where the

components of the spin-wave wave vector κ_{my} and κ_{nz} have discrete values due to the finite in-plane sizes of the rectangular magnetic element.

Another qualitative feature that distinguishes a rectangular element from an infinite film is the inhomogeneity of the internal field inside the element. This inhomogeneity leads to the different effective values of the internal field for the different spin-wave modes. These effective values of the field can be easily calculated using Eqs. (9) and (10) if the spatial distributions of the variable magnetization in a particular spin-wave mode $m_{mn}^2(\boldsymbol{\rho})$ are known.

The approximate equations defining discrete frequencies of the spin-wave eigenmodes of a rectangular magnetic element in this case can be written as[20]

$$\omega_{mn}^2 = (\omega_H^{mn} + \alpha\omega_M\kappa_{mn}^2)[\omega_H^{mn} + \alpha\omega_M\kappa_{mn}^2 + \omega_M F_{mn}(\kappa_{mn}L)],$$

$$(13)$$

where the quantity ω_H^{mn} (proportional to the effective value of the internal field for a particular spin-wave mode H_{mn}) is defined as

$$\omega_H^{mn} = \omega_H - \omega_M N_{mn},$$ (14)

where

$$N_{mn} = \frac{4}{wl}\int d\boldsymbol{\rho}\, m_{mn}^2(\boldsymbol{\rho})N_{zz}(\boldsymbol{\rho}).$$ (15)

The quantity $F_{mn}(\kappa_{mn}L)$ plays the role of a quantized matrix element of the dipole-dipole interaction

$$F_{mn}(\kappa_{mn}L) = 1 + P(\kappa_{mn}L)[1 - P(\kappa_{mn}L)]\left(\frac{\omega_M}{\omega_H^{mn} + \alpha\omega_M\kappa_{mn}^2}\right)$$
$$\times\left(\frac{\kappa_{my}^2}{\kappa_{mn}^2}\right) - P(\kappa_{mn}L)\left(\frac{\kappa_{nz}^2}{\kappa_{mn}^2}\right)$$ (16)

with $P(\kappa_{mn}L)$ defined by

$$P(qL) = 1 - \frac{1 - \exp(qL)}{qL}$$ (17)

and $\kappa_{mn}^2 = \kappa_{my}^2 + \kappa_{nz}^2$.

B. Spin-wave mode profiles and quantization conditions

To determine spatial distributions of the variable magnetization and quantized values of the wave vector projections κ_{my} and κ_{nz} in the spin-wave eigenmodes of a rectangular magnetic element we shall make a strong assumption, that a two-dimensional distribution of magnetization $m_{mn}(\boldsymbol{\rho}) = m_{m,n}(y,z)$ can be approximately factorized as follows:

$$m_{mn}(y,z) = \varphi_m(\kappa_{my}y)\mu_n(\kappa_{nz}z),$$ (18)

where functions φ_m are similar to the eigenfunctions of a longitudinally magnetized infinitely long stripe discussed in detail in Ref. 18, while the functions μ_n are similar to the eigenfunctions of a transversely magnetized infinitely long stripe considered in Refs. 19,20,38. Here κ_{my} and κ_{nz} are the quantized values of the corresponding components of the spin-wave wave vector, and $m,n=1,2,3,\ldots$. The approxi-

mate factorization (18) is justified by the fact that the inhomogeneity of the internal magnetic field in the rectangular element occurs mainly along the direction of this field (z direction), while the internal field is nearly constant along the y direction, as is shown in Fig. 2.

The spatial profiles of the functions $\varphi_m(\kappa_{my}y)$ and the quantized values of the wave vector projection κ_{my} perpendicular to the applied field are given by Eqs. (10) and (11) in Ref. 18. The situation with the functions $\mu_n(\kappa_{nz}z)$ and the discrete components of the wave vector κ_{nz} along the applied field (i.e., z direction) is more complicated. As was discussed in our previous papers, the spin-wave modes of a transversely magnetized magnetic element of a finite width can be of two distinct types: exchange-dominated modes localized near the stripe edges (see Refs. 9,10,19) and dipole-dominated modes localized near the stripe center (see Ref. 20). The one-dimensional spatial profiles along the z direction for both exchange-dominated and dipole-dominated spin-wave modes can be approximately evaluated using Eq. (12) in Ref. 19 and Eq. (12) in Ref. 20 correspondingly.

The spatial profiles of these modes can be also calculated numerically from Eq. (6) taken in the limit when the size w becomes infinitely large ($w \gg l$ or $w \to \infty$), while the size l (along the z direction) remains finite. In this particular case Eq. (6) becomes one dimensional

$$\left[-\alpha\omega_M\frac{d^2}{dz^2} + \omega_{H_i}\right]\hat{\mathbf{I}}\cdot\mathbf{m}(z) + i\omega\hat{\mathbf{T}}\cdot\mathbf{m}(z)$$
$$- \omega_M\int_{-l/2}^{l/2}dz'\hat{\mathbf{G}}_{x,y}(z,z')\mathbf{m}(z') = 0,$$ (19)

where the quantity $\omega_{H_i}(z) = \gamma H_i(z)$, proportional to the internal magnetic field $H_i(z)$, is dependent on the coordinate z along the stripe width l due to the static demagnetization. In fact, the static demagnetization problem in this case has been solved analytically by Joseph and Schlömann,[17] and the solution has the following form [analogous to Eq. (8)]:

$$H_i(z) = H_e - N_{zz}(z)4\pi M_S,$$ (20)

where

$$N_{zz}(z) = \frac{1}{\pi}\left[\arctan\left(\frac{L}{2z+l}\right) - \arctan\left(\frac{L}{2z-l}\right)\right].$$ (21)

The components of the tensorial Green's function $\hat{\mathbf{G}}_{x,y}$ in the considered case are given by the expressions

$$G_{xx}(z,z') = \frac{1}{2\pi L}\ln\left[\frac{(z-z')^2}{(z-z')^2 + L^2}\right],$$ (22)

$$G_{yy} = 0.$$ (23)

The nondiagonal components of the Green's function tensor vanish as one considers the averaged field across the stripe thickness.

The integral-differential equation (19) with a coordinate-dependent coefficient (internal field) (20) can be solved numerically to find the spin-wave eigenmodes $\mu_n(z)$. We solved this equation assuming unpinned surface spins at the top and
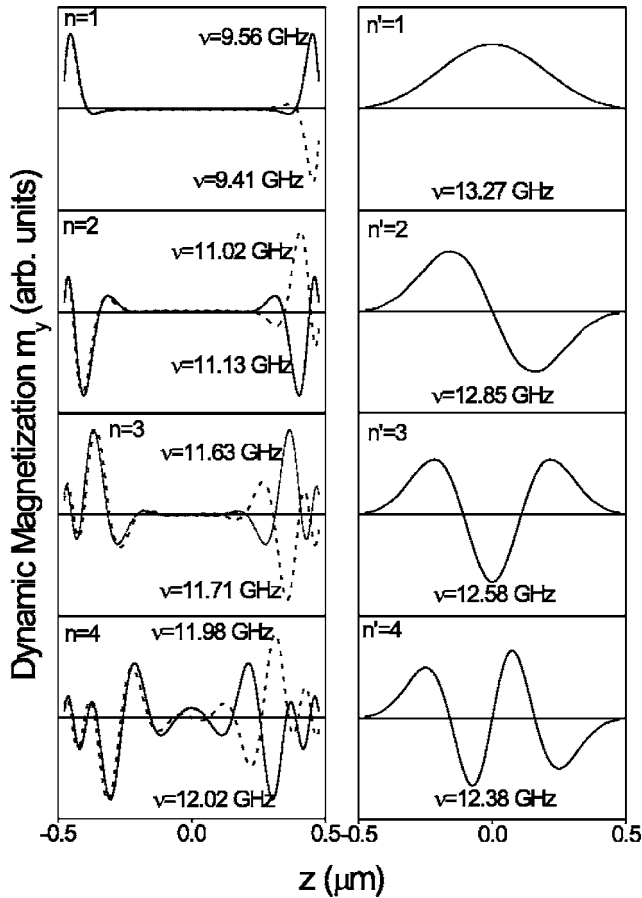
FIG. 6. Mode profiles and corresponding frequencies of a 1-μm-wide and 33-nm-thick stripe in an transversely applied magnetic field of 2000 Oe. The mode profiles $m_y(z)$ were obtained by solving Eq. (19) numerically. The index n denotes the exchange dominated modes while n' denotes the purely dipolar modes as explained in the text. Note, that two exchange-dominated modes corresponding to the same mode number n are nearly degenerate in frequency.
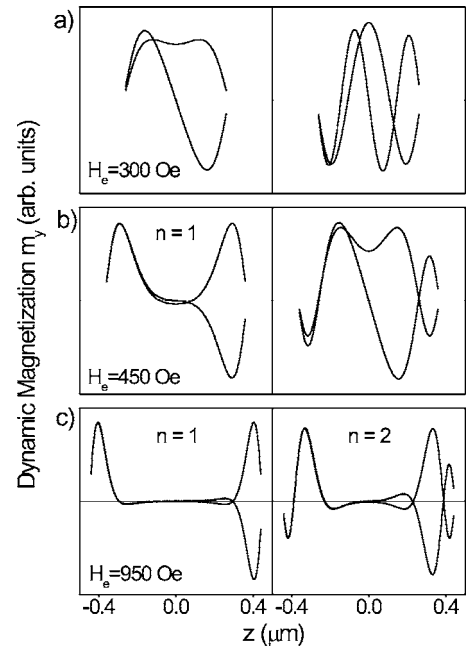

FIG. 7. Numerically calculated eigenfunctions $m_y(z)$ of the dynamic magnetization for the two lowest doublets of modes and for different applied fields (a) $H_e = 300$ Oe, (b) $H_e = 450$ Oe, (c) $H_e = 950$ Oe. The mode profiles are calculated in that region where the internal field is nonzero. The stripe was 1-μm wide and 33-nm thick.

bottom surfaces of the stripe $x = \pm L/2$ due to the absence of the surface anisotropy. We also assumed that due to negligible exchange surface anisotropy at the lateral edges of the stripe the boundary conditions for the variable magnetization are completely determined by the dipolar interaction. It turns out that these boundary conditions are very similar to the effective dipolar boundary conditions [see Eq. (8) in Ref. 18]. Also, since the stripe thickness L is much smaller than the stripe width l ($L \ll l$), for the lowest spin-wave modes these conditions are very close to the boundary conditions of total pinning of the variable magnetization at the edges $m|_{z = \pm l/2} = 0$. The boundary conditions for dynamic magnetization in thin magnetic elements that take into account inhomogeneous demagnetizing fields near element edges were recently calculated in Ref. 39

The eigenfunctions $\mu_n(z)$ of the variable magnetization m_y obtained from the numerical solution of Eq. (19) for the value of the external field equal to $H_e = 2000$ Oe are presented in Fig. 6. The spatial distributions of the component m_x are not shown as they are similar in shape, but one order of magnitude smaller due to the ellipticity of the precession.

It is evident from Fig. 6, that in the case of a strong external bias magnetic field numerical solution gives two distinct types of spin-wave modes in the spectrum: the exchange-dominated "edge" modes numbered with the index n and localized in the narrow spatial regions near the stripe edges, and quasi-cosinusoidal dipole-dominated modes numbered with the index n' and localized near the center of the stripe. Thus, the direct numerical solution of the dipole-exchange integral-differential equation (19) supports the conclusions of the earlier analytical theory presented in Refs. 9,10,19,20.

It should be mentioned, that a clear separation of the "exchange-dominated" modes ($n = 1, 2, 3, 4$) and "dipolar-dominated" modes ($n' = 1, 2, 3, 4, \ldots$) exists only in large bias fields $H_e > 1000$ Oe. At a smaller value of the applied bias field the modes have a mixed character which is illustrated by Fig. 7 where the profiles of the lowest modes of a stripe ($l = 1$ μm) are calculated from Eq. (19) for different values of the field H_e ($H_e = 300$, 450, and 950 Oe). As it is seen, for a field $H_e = 300$ Oe these modes have no pronounced "exchange" character and are not localized near the edges of the stripe. Therefore n is not a good quantum number in the low field range.

The quantization condition for the modes localized along the axis z has the integral form [see Eq. (3) in Ref. 9] and the evaluation of the discrete values of the wave vector component κ_{nz} for a particular mode is nontrivial. However, using Eq. (3) in Ref. 9 and the theorem estimating the mean value of an integral, we can approximately evaluate the characteristic wave vector of a localized mode as

$$\kappa_{nz} = \frac{n\pi}{\Delta z_n}, \tag{24}$$

where Δz_n is the localization length for a particular mode.

The characteristic localization lengths for both exchange-dominated (Δz^{ex}) and dipole-dominated (Δz^{dip}) spin-wave modes can be evaluated if the profile of the internal magnetic field along the axis z is known (see Fig. 3 in Ref. 9 for the evaluation of Δz^{ex} and Fig. 2 in Ref. 20 for the evaluation of Δz^{dip}).

As it was shown both theoretically and experimentally,[9–11] the localization length of an exchange-dominated spin-wave mode can be less than $\frac{1}{10}$ of a stripe width $\Delta z_1^{ex} < l/10$, so that the characteristic wave vector component of the mode along the direction of magnetization can be rather high, e.g., for $l = 1~\mu$m

$$\kappa_{1,z} = \frac{\pi}{\Delta z_1^{ex}}, \tag{25}$$

it can easily exceed the maximum value of the wave vector reachable by the BLS experiment (usually 2.5×10^5 cm^{-1}).

Analogously, we can calculate the quantized wave vector component for dipole-dominated localized modes

$$\kappa_{n'=1,z} = \frac{\pi}{\Delta z_1^{dip}}, \tag{26}$$

where $\Delta z_{n'}^{dip}$ is the localization length for a dipolar localized mode. This dipolar localization length for the lowest dipolar mode Δz^{dip} is, usually, between l and $l/2$.

For the modes in small external bias fields, when the influence of dipolar and exchange interactions are comparable, this approximation, of course, cannot be applied (see, e.g., Fig. 7 for $H_e = 300$ Oe). Using the approximate eigenfunctions (18) and quantized values of the wave vector components κ_{my} and κ_{nz} calculated from Eq. (11) in Ref. 18 and Eq. (24), correspondingly and the approximate equation for the mode frequency Eq. (13) we can calculate the eigenfrequencies of the spin-wave modes of a rectangular magnetic element.

We calculated these eigenfrequencies for a rectangular permalloy element investigated in our experiment (Fig. 3). We used the following parameters of the element in our calculation: thickness $L = 33$ nm, lateral sizes $l \times w = 1.75 \times 1~\mu$m^2, $4\pi M_S = 10.2$ kOe, exchange constant $\alpha = 2.5 \times 10^{-13}$ cm^2, or $A \simeq 1 \times 10^6$ erg/cm^3, $H_e = 600$ Oe, gyromagnetic ratio for the electron $\gamma/2\pi = 2.97$ MHz/Oe. The magnetic parameters were determined independently from experiments on unsaturated films.

The lowest $n = 1$, $m = 1$ mode having the frequency of 4.9 GHz was identified as an exchange-dominated mode, localized near the element edges that are perpendicular to the external bias magnetic field. The localization length of this mode along the direction of the magnetic field (z direction) was evaluated as $\Delta z_1^{ex} = 0.3~\mu$m. For simplicity the spatial distribution of this exchange-dominated localized mode within the region of its localization was assumed to be cosinusoidal

TABLE I. Comparison of frequencies (in GHz) of eigenmodes in a rectangle obtained from experiment and different theoretical techniques.

experiment	mode index	analytic theory	Langevin dynamics	OOMMF
5.2–5.6	($m=1, n=1$)	4.9	4.94	4.3
7.1–8.2	($m=1, n'=1$)	8.6	7.98–8.11	8.2
10.0–10.4	($m=2, n'=1$)	10.6	10.52–10.65	
12.0–12.7	($m=3, n'=1$)	12.1	12.55–12.67	11.7
13.2–13.9	($m=4, n'=1$)	13.1	not observed	
14.5–14.8	($m=5, n'=1$)	14.0	13.94	13.6
	($m=6, n'=1$)	14.7	14.57–14.70	

$$\mu_{n=1}(\kappa_{1z}^{ex}z) = \cos\left(\frac{\pi}{\Delta z_1^{ex}}(z - l^*/2)\right) \tag{27}$$

in the intervals $l^*/2 - \Delta z_1^{ex} \leqslant |z| \leqslant l^*/2$ and zero elsewhere (i.e., in the interval $|z| < l^*/2 - \Delta z_1^{ex}$). Here the effective length of the magnetic element $l^* < l$ is the length of the region where the internal bias magnetic field is positive.

For all the other experimentally observed modes we assumed that the distribution along the z direction is similar to the lowest dipole-dominated localized mode (mode $n' = 1$ in Fig. 6). For the experimental conditions ($H_e = 600$ Oe) the localization length of this distribution was evaluated as $\Delta z_1^{dip} = 0.85~\mu$m. The spatial distribution of this lowest dipole-dominated mode along the z direction was also assumed to be cosinusoidal

$$\mu_{n'=1}(\kappa_{1z}^{dip}z) = \cos\left(\frac{\pi}{\Delta z_1^{dip}}z\right) \tag{28}$$

in the interval $|z| \leqslant \Delta z_1^{dip}/2$ and zero elsewhere (i.e., in the interval $\Delta z_1^{dip}/2 < |z| < l/2$).

The magnetization distributions of both exchange-dominated and dipole-dominated modes along the y direction were assumed to be described by Eq. (10) in Ref. 18. The two-dimensional spatial distribution of the variable magnetization in these analytically calculated modes are shown in the right panel of Fig. 10 while their calculated frequencies are given in the third column of the Table I.

V. MICROMAGNETIC SIMULATIONS AND DISCUSSION

To check the validity of the above described results obtained in the framework of the approximate analytical approach, we performed micromagnetic simulations of the dynamic properties of rectangular magnetic elements. The commercially available micromagnetic packages MICROMAGUS (Ref. 40) and OOMMF (Ref. 21) have been employed to produce "raw" simulation data, i.e., spin precessions at the different points of the sample. To calculate the excitation spectra further processing of the data was performed, as described below.

The first set of numerical simulations was performed using the MICROMAGUS package.[40] In the MICROMAGUS pack-

age a system magnetization dynamics is simulated using the standard extension of the Landau-Lifshitz-Gilbert (LLG) equation of motion for magnetic moments which includes finite-temperature random fluctuations

$$\frac{d\mathbf{M}_i}{dt} = -\gamma[\mathbf{M}_i \times (\mathbf{H}_i^{\text{det}} + \mathbf{H}_i^{\text{fl}})]$$
$$-\gamma\frac{\lambda}{M_S}\{\mathbf{M}_i \times [\mathbf{M}_i \times (\mathbf{H}_i^{\text{det}} + \mathbf{H}_i^{\text{fl}})]\}, \quad (29)$$

where the precession constant γ (>0) is equal to the gyromagnetic ratio of the spins for small dissipation $\lambda \ll 1$, and the deterministic field $\mathbf{H}_i^{\text{det}}$ acting on each magnetic moment $\mathbf{M}_i$ includes all standard micro-magnetic interactions: external, anisotropy, exchange, and dipolar fields.

The fluctuation (or Langevin) field $\mathbf{H}_i^{\text{fl}}$ is introduced to take into account random thermal noise responsible for spontaneous fluctuations of the system magnetization for finite temperatures. The question concerning the statistical properties of this random field is crucially important for obtaining correct physical results from numerical simulations. Hence we will briefly address this question here leaving a detailed methodological explanation to a separate publication.

To the best of our knowledge, in virtually all micromagnetic simulations the simplest statistical properties of its Cartesian components of the fluctuation field

$$\langle H_{\xi,i}^{\text{fl}}(t)\rangle = 0, \quad (30)$$

$$\langle H_{\xi,i}^{\text{fl}}(0)H_{\psi,j}^{\text{fl}}(t)\rangle = 2D\delta(t)\delta_{ij}\delta_{\xi\psi} \quad (31)$$

were used [here indices i,j refer to discretization cells, $\xi,\psi = x,y,z$ and the noise power $D = \lambda/(1+\lambda^2)$ ($kT/\gamma M$) is proportional to the system temperature T]. The relation (31) was rigorously derived from the fluctuation-dissipation theorem in Ref. 41 for a system of noninteracting single-domain particles (actually for point dipoles with a uniaxial on-site anisotropy), so that the usage of the same simple correlation properties for a much more complicated micromagnetic system requires careful justification.

First of all, we point out that the sole presence of the interactions between elementary system moments (representing the magnetization vectors in finite element discretization cells) does *not* require the introduction of non-trivial correlations between the random field components, because these interactions are taken into account via the deterministic part of the effective field $\mathbf{H}_i^{\text{det}}$ in Eq. (29). The corresponding generalization of the fluctuation-dissipation theorem for a system of interacting magnetic moments can be found in Ref. 44.

However, in micromagnetic simulations there exist, in principle, at least three reasons to use more complicated random field correlations than those given by Eq. (31). The first reason—the physical one—is the presence of correlations of thermal bath phonon fluctuations (supposed to cause the magnetization fluctuations). Their exact correlation properties are not known. However, since the system is considered to be at a room temperature, i.e., at a temperature comparable to the Debye temperature of the lattice, it is reasonable to

suggest that these correlations are short range (in space and time) and have an exponentially decaying correlation function. Hence, the δ-functional expression (31) can be used as a good first approximation for these correlations, providing that we are interested in processes whose characteristic time and space scales are much larger than the corresponding decay time (picoseconds, i.e., $2\pi/\omega_D$, where ω_D is the Debye frequency) and the correlation length (several interatomic distances) of the heat bath fluctuations.

The other two reasons are due to the finite-difference approximation of the continuous micromagnetic problem. First of all, such an approximation does not allow one to take into account magnetic excitations with a wavelength smaller than the grid cell size Δx. However, due to magnon-magnon interactions such magnons can excite a precession of the cell magnetic moment. Since they can have a mean free path which is much larger than Δx, they can cause substantial correlations of the effective fields acting on the magnetic moments of the neighboring cells (see Ref. 42 for details). Whether these correlations are important for the particular magnetization dynamics under study can be determined comparing simulation results for grids with various cell sizes. We have checked that in our case these correlations do not play any significant role as soon as the grid cell is smaller than the exchange correlation length $\Delta x < l_{\text{ex}} = \sqrt{A/2\pi M_S^2}$ (where A denotes the exchange constant and M_S the material saturation magnetization).

The qualitative change in the density of magnon states (m-DOS) due to the transition from the formally continuous (discrete on the atomic scale) to a finite element micromagnetic system is the third reason why more complicated correlations of the random field than those given by Eq. (31) should, in principle, be used. However, we show elsewhere[43] that for frequencies much less than the frequency of the van Hove singularity in the m-DOS for the discretized (not initial) system this effect can also be neglected. This is the case for the current study. Based on the discussion above, we used in our micromagnetic simulations the δ-correlated noise $\mathbf{H}_i^{\text{fl}}$.

The spectrum of magnetic eigenmodes in Permalloy elements was simulated in the following way. The rectangular Permalloy element with lateral sizes $l \times w = 1.75 \times 1~\mu\text{m}^2$ and the thickness $L = 33$ nm (as used in our BLS experiments) was discretized using a grid with $N_x \times N_z \times N_y = 4 \times 180 \times 100$ cells; it was checked on a smaller system that further grid refinement did not lead to any noticeable changes in the magnon spectrum for the frequency range studied here (except for the lowest mode—see below). Periodic boundary conditions were applied with the distance between the Permalloy elements equal to the experimental spacing $\Delta = 100$ nm.

In our simulations we used the same material parameters for Permalloy as in the above described analytical calculation. The cubic crystallographic anisotropy of Permalloy ($K_{\text{cub}} = 5 \times 10^3$ erg/cm^3) was proven to be too low to have any influence on the simulation results and hence was neglected. The dissipation constant was set to $\lambda = 0.01$.

Minimizing the micromagnetic energy of the permalloy element starting from the state with the corresponding symmetry, we found that in the external field $H_e = 600$ Oe used in the experiment three types of the magnetization configura-
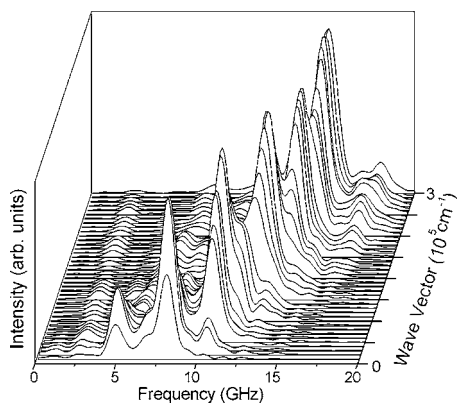
FIG. 8. Power spectra of the m_x oscillations for a sequence of in-plane wave vectors $q_\perp$ perpendicular to the field direction (and to the long side of the Py element) obtained using Langevin dynamics simulations (Ref. 40).

tion for $T=0$ are possible: the so called S, C, and flower states. Among them we have used the S-type magnetization state as the initial state, because the flower state was found to be unstable with respect to thermal fluctuations. By the equilibration of the system at room temperature $T=300$ K this state switched to either S or C states. Magnon spectra for the C state were identical to the S-state spectra up to the accuracy of small frequency shifts of the lowest mode near the domain walls between the closure and central domains.

After the initial magnetization configuration was obtained, dynamical simulations using Eq. (29) were performed. The system temperature was set to be equal to room temperature $T=300$ K. To obtain the magnon spectrum in the thermodynamical equilibrium, the system was first equilibrated by integrating Eq. (29) until the system energy has stopped to increase in frames of statistical errors (the "heating" phase). Afterwards time dependences of all the grid cell moments were recorded with the sampling interval Δt_{min} $=1$ ps which provided a sufficiently good statistics to determine spectra up to the maximum frequency ν_{max} $\sim 0.1/\Delta t_{min}=100$ GHz. To achieve the required lowest frequency $\omega_{min}/2\pi \sim 5$ GHz simulations were performed for the total time $\Delta t_{min}=5 \times 2\pi/\omega_{min}=1$ ns. The resulting spectra (see Fig. 8) were obtained using Fourier analysis of the recording time dependences by averaging over at least N_{run} $=8$ independent simulation runs. The calculated magnon spectra are shown in Fig. 8. The eigenmodes manifest themselves as sequences of peaks having the same frequency for several subsequent wave vectors. The numerical values of the magnon eigenfrequencies calculated in this Langevin dynamics simulation are presented in column 4 of Table I.

For the computation of the spatial distribution of the oscillation power of a magnetization component $m_{(x,y,z)}$ for the given frequency $\omega/2\pi$ we first performed the time Fourier transforms of $m_{(x,y,z)}$-time dependences for all discretization cells, thus obtaining the spectral power as a function of the frequency for all cells. Then we used the spectral power values for the required frequency $\omega_0/2\pi$ (extracted from all these spectra) to build up the corresponding spatial maps (see Fig. 9).

The spatial distributions of static magnetization in the rectangular magnetic element and the spatial distribution of
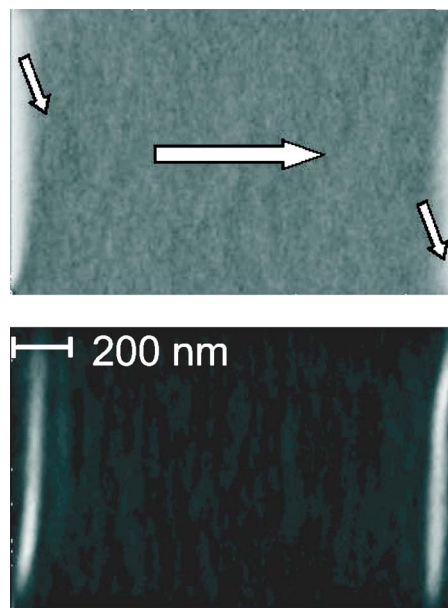

FIG. 9. Upper panel: Distribution of static magnetization used for Langevin dynamics. Lower panel: Spatial distribution of the lowest exchange-localized mode having a frequency of 4.94 GHz.

the dynamic magnetization in the lowest oscillation mode obtained using the method of Langevin dynamics are shown in the lower and upper panels of Fig. 9, correspondingly. As it is evident from the right panel of Fig. 9 the lowest magnon mode with the smallest frequency of 4.94 GHz corresponds to the oscillations in the region of inhomogeneous internal field near the domain walls of the closure domains in our S structure, which supports the conclusions obtained using the approximate analytical approach.

Also, for all the oscillation modes the regions where the oscillation power is concentrated are extended along the short side of the magnetic element (perpendicular to the applied field direction). This feature explains the experimental observation Fig. 4 that the corresponding spectra of the magnon excitations in the wave vector space show a pronounced peak along the direction perpendicular to the internal field (y direction), but is extended over the whole measured wave vector range for the direction parallel to the internal magnetic field (z direction).

The second set of micromagnetic simulations was performed using the object-oriented micromagnetic framework[21] (OOMMF). In this simulation the stripe was discretized along the y and z directions with a cell size of 5 nm. The initial condition for the dynamic simulation was obtained by relaxing from a state of homogeneous magnetization $M_S \mathbf{e}_x$ with a large Gilbert damping parameter $\lambda=0.5$. In contrast to the results obtained using MICROMAGUS, the flower state is stable in OOMMF and, therefore, it was used as an initial condition. The reasons for that might be that (i) the simulations performed using OOMMF do not take into account thermal fluctuations (which corresponds to $T=0$), (ii) the element was not discretized into sublayers, and (iii) in the simulations with MICROMAGUS periodic boundary conditions were employed what might favor the S state.

The dynamical calculation was undertaken with a smal damping parameter of $\lambda=0.01$ so that the magnetization os-
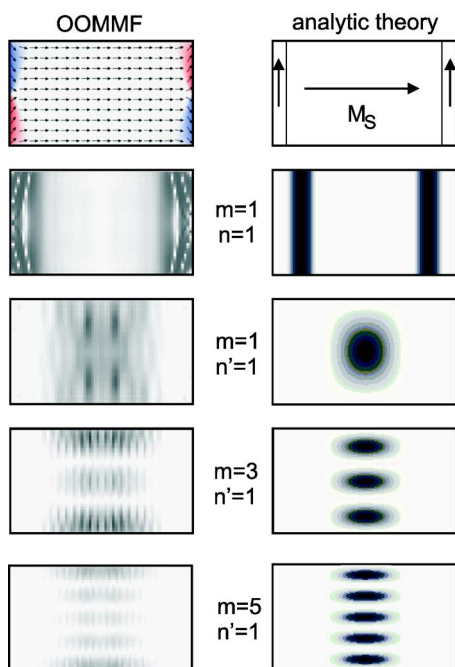
FIG. 10. Comparison of OOMMF with analytic theory for several modes. The upper graphs show the static equilibrium magnetization used in the two models. The corresponding effective field is shown in Fig. 2.

cillations could be observed over several periods. The eigenfrequencies did not depend significantly on the damping. A uniform Gaussian field pulse with a full-width at half maximum (FWHM) of 150 ps and an amplitude of 10 Oe was applied in the x direction, and the response over the next 10 ns was calculated using 10 ps time steps during the pulse and 20 ps steps after the pulse.

A local Fourier transform was performed with these time domain data and power spectral images as a function of the frequency were computed. All images are normalized by the total spectral weight at each position. A more detailed discussion of this procedure can be found in Refs. 11,33. Adding all the local Fourier transform data one obtains a so-called integrated Fourier transform. In this integrated Fourier transform several distinct peaks corresponding to the spin-wave modes can be observed.

The left panel in Fig. 10 shows the power spectral images (or spatial power distributions) for several frequencies corresponding to the maxima in the integrated Fourier transform that were calculated using OOMMF. The spatial distributions of the spin wave modes calculated using the approximate analytical approach are shown in the right panel of Fig. 10.

Note, that the OOMMF approach accounts only for the modes whose mean value of the dynamical magnetization is non zero, i.e., modes with an even number of nodes (m = 1, 3, 5, ...), since the precession in our numerical simulation was excited by a spatially uniform field pulse. The small-wavelength noise is due to the fact that the cell size is in the order of the exchange correlation length but not substantially smaller. The mode ($m=1, n'=1$) in Fig. 10 corresponds rather to a band of non-resolved modes with a broad frequency peak, while the modes with higher $m>1$ are

well defined in frequency. The values of the mode frequencies calculated using OOMMF are presented in column 5 of Table I.

Table I contains the values of the frequencies of the spin-wave eigenmodes of a rectangular magnetic element measured in our BLS experiment (see Fig. 3) and calculated by two different numerical and one approximate analytical method. It is evident that all the used theoretical methods give a reasonably good quantitative description of the experimental data and, also, are in a surprisingly good agreement among themselves. The only exception is the lowest eigenmode. We believe that the difference between the simulated and experimentally measured frequencies for this mode can be attributed to the fact that the discretization into the $N_\perp$ =4 layers performed in the Langevin dynamics numerical approach in the direction perpendicular to the layer plane is insufficient to resolve the structure of the domain wall fine enough to reproduce correctly its exact oscillation behavior of magnetization in this mode. We would like also to note that there were no adjustable parameters for both sets of our numerical simulations.

It is also worth noting, that the spatial distributions of the spin-wave eigenmodes obtained using different theoretical methods are qualitatively similar (compare Figs. 10 and 9) which demonstrates once again that the ideas of the spin-wave mode structure in a thin rectangular magnetic element obtained using our simple approximate analytical approach were qualitatively correct.

VI. CONCLUSION

In summary we studied both experimentally and theoretically the discrete spin-wave eigenmodes of thin rectangular magnetic elements having two finite in-plane dimensions and magnetized parallel to one of the element sides. We demonstrated that the effects of lateral confinement drastically affect the properties of the magnetic eigenmodes in those elements. The spin-wave eigenmodes of a rectangular element turn out to be not only quantized due to the finite in-plane dimensions, but also localized due to the inhomogeneity of the internal bias magnetic field. We also demonstrated that the approximate analytic theory of the spectrum of these eigenmodes based on the dispersion equation for spin waves in an infinite magnetic film gives the results that are in good quantitative agreement with both the results of micromagnetic numerical simulations and the results of the BLS experiments.

*Electronic address: cbayer@physik.uni-kl.de

[1] *The Physics of Ultra-High-Density Magnetic Recording*, edited by M. L. Plumer, J. van Ek, and D. Weller (Springer, Berlin, 2001).

[2] *Spindynamics in Confined Magnetic Structures I*, edited by B. Hillebrands and K. Ounadjela (Springer, Berlin, (2002); *Spindynamics in Confined Magnetic Structures II*, edited by B. Hillebrands and K. Ounadjela, (Springer, Berlin, 2003).

[3] B. A. Gurney, P. Baumgart, V. S. Speriosu, R. E. Fontana, A. Patlac, A. Logan, and P. Humbert, (unpublished).

[4] C. Mathieu, C. Hartmann, M. Bauer, O. Büttner, S. Riedling, B. Roos, S. O. Demokritov, B. Hillebrands, B. Bartenlian, C. Chappert, D. Decanini, F. Rousseaux, E. Cambril, A. Müller, B. Hoffmann, and U. Hartmann, Appl. Phys. Lett. **70**, 2912 (1997).

[5] C. Mathieu, J. Jorzick, A. Frank, S. O. Demokritov, B. Hillebrands, A. N. Slavin, B. Bartenlian, C. Chappert, D. Decanini, F. Rousseaux, and E. Cambril, Phys. Rev. Lett. **81**, 3968 (1998).

[6] J. Jorzick, S. O. Demokritov, C. Mathieu, B. Hillebrands, B. Bartenlian, C. Chappert, F. Rousseaux, and A. N. Slavin, Phys. Rev. B **60**, 15 194 (1999).

[7] Y. Roussigné, S. M. Chérif, C. Dugautier, and P. Moch, Phys. Rev. B **63**, 134429 (2001).

[8] Z. K. Wang, M. H. Kuok, S. C. Ng, D. J. Lockwood, M. G. Cottam, K. Nielsch, R. B. Wehrspohn, and U. Gösele, Phys. Rev. Lett. **89**, 027201 (2002).

[9] J. Jorzick, S. O. Demokritov, B. Hillebrands, D. Berkov, N. L. Gorn, K. Guslienko, and A. N. Slavin, Phys. Rev. Lett. **88**, 047204 (2002).

[10] C. Bayer, S. O. Demokritov, B. Hillebrands, and A. N. Slavin, Appl. Phys. Lett. **82**, 607 (2003).

[11] J. P. Park, P. Eames, D. M. Engebretson, J. Berezovsky, and P. A. Crowell, Phys. Rev. Lett. **89**, 277201 (2002).

[12] N. Smith and P. Arnett, Appl. Phys. Lett. **78**, 1448 (2001).

[13] J.-G. Zhu, J. Appl. Phys. **91**, 7273 (2002).

[14] Y. Zhou, A. Roesler, and J.-G. Zhu, J. Appl. Phys. **91**, 7276 (2002).

[15] C. Kittel, Phys. Rev. **73**, 2 (1948).

[16] L. R. Walker, Phys. Rev. **105**, 2 (1957).

[17] R. I. Joseph and E. Schlömann, J. Appl. Phys. **36**, 1579 (1965).

[18] K. Yu. Guslienko, S. O. Demokritov, B. Hillebrands, and A. N. Slavin, Phys. Rev. B **66**, 132402 (2002).

[19] G. Gubbiotti, M. Conti, G. Carlotti, P. Candeloro, E. Di Fabrizio, K. Yu. Guslienko, A. Andre, C. Bayer, and A. N. Slavin, J. Phys.: Condens. Matter **16**, 7709 (2004).

[20] K. Y. Guslienko, R. W. Chantrell, and A. N. Slavin, Phys. Rev. B **68**, 024422 (2003).

[21] M. J. Donahue and D. G. Porter, *OOMMF User's Guide, Version 1.0*, in Interagency Report No. NISTIR 6376 (National Institute of Standards and Technology, Gaithersburg, Maryland, 1999).

[22] M. Grimsditch, G. K. Leaf, H. G. Kaper, D. A. Kapreev, and R. E. Camley, Phys. Rev. B **69**, 174428 (2004).

[23] M. Grimsditch, L. Giovannini, F. Montoncello, F. Nizzoli, G. K. Leaf, and H. G. Kaper, Phys. Rev. B **70**, 054409 (2004).

[24] L. Giovannini, F. Montoncello, F. Nizzoli, G. Gubbiotti, G. Carlotti, T. Okuno, T. Shinjo, and M. Grimsditch, Phys. Rev. B **70**, 172404 (2004).

[25] B. Heinrich, R. Urban, and G. Woltersdorf, J. Appl. Phys. **91**, 7523 (2002).

[26] W. K. Hiebert, A. Stankiewicz, and M. R. Freeman, Phys. Rev. Lett. **79**, 1134 (1997).

[27] A. Barman, V. V. Kruglyak, R. J. Hicken, J. M. Rowe, A. Kundrotaite, J. Scott, and M. Rahman, Phys. Rev. B **69**, 174426 (2004).

[28] Y. Acremann, C. H. Back, M. Buess, O. Portmann, A. Vaterlaus, D. Pescia, and H. Melchior, Science **290**, 492 (2000).

[29] B. Hillebrands, Rev. Sci. Instrum. **70**, 1589 (1999).

[30] P. Bryant and H. Suhl, Appl. Phys. Lett. **54**, 2224 (1989).

[31] M. J. Donahue, D. G. Porter, R. D. McMichael, and J. Eicke, J. Appl. Phys. **87**, 5520 (2000).

[32] B. A. Kalinikos, A. N. Slavin, J. Phys. C **19**, 7013 (1986).

[33] C. Bayer, J. P. Park, H. Wang, M. Yan, C. E. Campbell, P. A. Crowell, Phys. Rev. B **69**, 134401 (2004).

[34] M. Bailleul, D. Olligs, and C. Fermon, Phys. Rev. Lett. **91**, 137204 (2003).

[35] Y. Roussigné, S. M. Chérif, and P. Moch, J. Magn. Magn. Mater. **263**, 289 (2003).

[36] Y. Roussigné, S. M. Chérif, and P. Moch, J. Magn. Magn. Mater. **268**, 89 (2004).

[37] K. Yu. Guslienko and A. N. Slavin, Mater. Sci. Forum **373–376**, 217 (2001).

[38] P. H. Bryant, J. F. Smyth, S. Schultz, and D. R. Fredkin, Phys. Rev. B **47**, 11 255 (1993).

[39] K. Y. Guslienko and A. N. Slavin, Phys. Rev. B (to be published).

[40] D. V. Berkov, N. L. Gorn, URL: http://www.micromagus.de

[41] W. F. Brown, Jr., Phys. Rev. **130**, 1677 (1963).

[42] D. V. Berkov and N. L. Gorn, J. Magn. Magn. Mater. **272–276P1**, 687 (2004).

[43] D. V. Berkov and N. L. Gorn, J. Magn. Magn. Mater. **290–291P1**, 442 (2005).

[44] H.-B. Braun, in *Structure and Dynamics of Heterogeneous Systems*, edited by P. Entel and D. Wolf (World Scientific, Singapore, 2000).